Dynamic electrostatic force microscopy in liquid media

G. Gramse,[1,2] M. A. Edwards,[1,a)] L. Fumagalli,[1,2] and G. Gomila[1,2,b)]
[1]*Nanobioelec Group, Institute for BioEngineering of Catalonia (IBEC), c/Baldiri i Reixac 15-21, 08028 Barcelona, Spain*
[2]*Departament d'Electrònica, Universitat de Barcelona c/Martí i Franquès 1, 08028 Barcelona, Spain*

We present the implementation of dynamic electrostatic force microscopy in liquid media. This implementation enables the quantitative imaging of local dielectric properties of materials in electrolyte solutions with nanoscale spatial resolution. Local imaging capabilities are obtained by probing the frequency-dependent and ionic concentration-dependent electrostatic forces at high frequency (>1 MHz), while quantification of the interaction forces is obtained with finite-element numerical calculations. The results presented open a wide range of possibilities in a number of fields where the dielectric properties of materials need to be probed at the nanoscale and in a liquid environment. © 2012 American Institute of Physics. [http://dx.doi.org/10.1063/1.4768164]

One of the distinguishing characteristics of atomic force microscopy (AFM) is the ability to investigate nanoscale phenomena in a liquid environment. This has made it an invaluable instrument for *in-situ* imaging and characterization in liquids, with a great impact in biology[1,2] and electrochemistry,[3,4] among others.

A variety of electrical material properties can be determined in liquids using AFM-based techniques, including electrochemical activity,[3] electromechanical response,[5,6] and surface charges and potentials[7–11] using both static and dynamic measuring modes. Yet, great difficulties still remain in probing and quantifying dielectric properties in a liquid environment in spite of the number of techniques available in air for such purposes: e.g., scanning capacitance microscopy,[12–15] scanning polarization force microscopy,[16] scanning impedance microscopy,[17,18] scanning microwave microscopy,[19] or electrostatic force microscopy (EFM).[20–22]

Measuring dielectric polarization phenomena at the nanoscale in electrolyte solutions is extremely challenging due to the complex frequency-dependent response of the solid-electrolyte interface, as well as large stray capacitance contributions that prevent access to local material dielectric properties. However, assessing dielectric properties of material surfaces in electrolyte solutions is fundamental to the understanding of a broad variety of electric phenomena. For example, in the fields of electrophysiology and electrochemistry, dielectric information could shed new light on the nanoscale properties of processes such as ion transport across membranes or metal corrosion allowing *in situ* discrimination between different oxides.

In this article, we present a method that extends electrostatic force microscopy to the liquid environment. We show that by combining high-frequency (>1 MHz) electrostatic force detection and finite-element numerical calculations, local and quantitative dielectric contrast in electrolyte solutions can be obtained with nanoscale spatial resolution.

High-frequency detection is the key to achieving nanoscale locality, as only then are the electrostatic forces acting on the tip sensitive to the local dielectric properties of the sample. We unambiguously demonstrate this by imaging and quantifying, in electrolyte solution, the dielectric constant of a 20 nm thick film of silicon dioxide at various frequencies.

The experimental setup that enables simultaneous topographical and dielectric measurements in liquid is shown schematically in Figure 1. It consists of an AFM in which a sinusoidal voltage signal, with an angular frequency ω_{el} in the MHz range and an amplitude modulated (AM) at angular frequency ω_{mod} in the kHz range, is applied between a conductive probe and the bottom of the sample, both in liquid environment. The high-frequency voltage, well beyond the mechanical resonance of the cantilever, bends the cantilever in a static way due to the non-linear dependence of the actuation force on the applied voltage. We modulated this force at a the lower-frequency, ω_{mod}, thus enabling ac detection by the lock-in amplifier with enhanced signal-to-noise ratio with respect to static detection.

To avoid electric double layer (EDL) interactions, we took the dielectric images by scanning the probe at distances much larger than the Debye length (typically 10 nm in 1 mM monovalent electrolytes). This experimental setup is able to probe *local* dielectric properties of materials in electrolyte solutions since in the MHz frequency range the frequency-dependent force acting on the probe becomes localized to the tip apex. Indeed, in an electrolyte solution, the electric force acting on the conducting probe in response to an ac applied voltage $v(t) = v_0 \cdot \sin(\omega t)$ is given by[23]

$$F_{elec}(z,t) = \frac{1}{2}\frac{\partial C_{sol}(z)}{\partial z} v_{sol}^2(z,t), \quad (1)$$

where C_{sol} is the capacitance of the solution gap between probe and sample—separated by a distance z not including the Debye layer contributions—and v_{sol} is the voltage drop across C_{sol}. From the analysis of the equivalent circuit of the probe-solution-sample system given in the inset in Figure 1, one finds that v_{sol}, and hence the electrostatic force, depends, among other parameters, on the dielectric properties of the
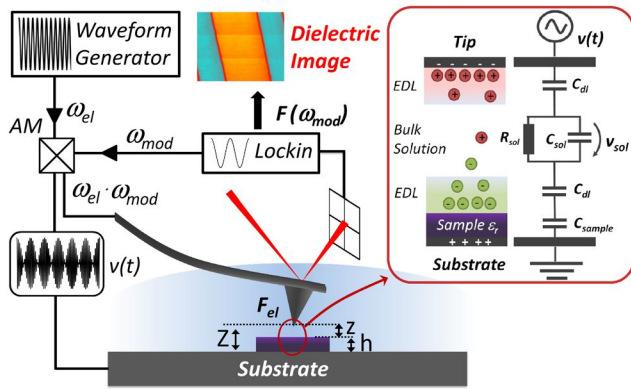

FIG. 1. EFM setup for measuring local dielectric properties of materials in electrolyte solution. An AM ac-potential with frequency ω_{el} ($>$ MHz) and modulation frequency ω_{mod} ($<$10 kHz) is applied between a conductive tip and a substrate in an electrolyte solution. An external lock-in amplifier detects the modulated bending of the cantilever. The cantilever bending depends, among other factors, on the local dielectric properties of the sample, which we mapped by scanning the tip at constant-height, Z, with respect to the substrate. Inset: Electrochemical model and equivalent circuit of a surface element of the tip-sample interaction region in solution, where C_{dl} is the double-layer capacitance, R_{sol} the solution resistance, C_{sample} the sample capacitance, $v(t)$ the applied voltage, and v_{sol} the solution's voltage drop.

sample. It is detectable only for frequencies higher than a critical frequency, f_{act}, given by $f_{act}^{-1} = 2\pi R_{sol}(C_{eq} + C_{sol})$, where R_{sol} is the solution resistance and C_{eq} is given by $C_{eq} = C_{dl} \cdot C_{sample}/(C_{dl} + 2C_{sample})$ with C_{sample} and C_{dl} the sample and double-layer capacitances, respectively. By assuming a parallel-plate model and neglecting the double-layer capacitances, we can roughly estimate f_{act} as

$$f_{act} = \frac{c \cdot \Lambda}{2\pi \cdot \varepsilon_0 \cdot \varepsilon_{r,water}} \left(\frac{\varepsilon_{r,sample}z}{\varepsilon_{r,water}h} + 1 \right)^{-1}$$

$$\approx 3\,\text{MHz} \times c(\text{mM}) \left(\frac{\varepsilon_{r,sample}z}{\varepsilon_{r,water}h} + 1 \right)^{-1}, \qquad (2)$$

where c is the solution electrolyte concentration, Λ the molar conductivity, h the thickness of the sample, $\varepsilon_{r,water} = 78$ is the dielectric constant of water, $\varepsilon_{r,sample}$ the dielectric constant of the sample, and z the distance between the sample and the tip (or the cantilever). Assuming typical experimental parameters, i.e., $\Lambda = 13.3\,\text{S}\ \text{m}^{-1}\ \text{mol}^{-1}$, $c = 1\,\text{mM}$, $h = 10\,\text{nm}$ and $\varepsilon_r = 4$, and taking $z = z_0 = 10\,\text{nm}$ for the tip-sample distance and $z = H + z_0$ for the cantilever-sample distance, where $H = 10\,\mu\text{m}$ is the cone height of the tip, we obtain $f_{act,tip} = 3\,\text{MHz}$ and $f_{act,cant} = 60\,\text{kHz}$ for the tip and cantilever, respectively. Therefore, electrical actuation of the cantilever can be obtained in electrolyte solutions for frequencies $\omega_{el}/2\pi = f > f_{act,cant} \approx \text{kHz}$, but local dielectric contrast can only be measured when $f > f_{act,apex} \approx \text{MHz}$. These results remain qualitatively correct when the realistic tip geometry is considered.

To validate this prediction, we measured a test structure consisting of thin stripes of silicon dioxide (20 nm thick and 2.5 μm wide) purchased from AMO GmbH. Experiments were performed using a commercial AFM (Nanotec Electronica SL) equipped with a custom-made liquid cell for electrical measurements made from Teflon and sealed by apiezon-wax. Solid platinum tips (Rocky Mountain Nanotechnology LLC)

with a spring constant of $k \sim 0.3\,\text{N/m}$ and resonance frequency in solution of $\sim 6\,\text{kHz}$ were used. All solutions were prepared from MilliQ (Merck Millipore) and $KClO_4$ (99.99% purity, Sigma Aldrich). We used an Agilent 33250 A as external waveform generator in amplitude modulation mode. The modulation signal came from an external Anfatec eLockIn 204/2. Figure 2(a) shows a topographic image of the SiO_2/Si microstructure in aqueous electrolyte solution obtained in conventional intermittent contact mode. The dielectric images were obtained subsequently in solutions of two electrolyte concentrations, 1 mM (Figure 2(b)) and 10 mM (Figure 2(c)). The tip was scanned at a constant height (Z = 100 nm) above the basal plane of the substrate and the frequency of the applied voltage, f, was changed every 10 lines from 20 MHz (top) to 100 kHz (bottom).

The higher-frequency dielectric images faithfully reproduce the periodic band structure of the substrate, thus clearly demonstrating the measurement is sensitive to local dielectric properties of the 20 nm-thick SiO_2 bands in electrolyte solutions. The local contrast is obtained only for applied frequencies above a given characteristic value, $f > 100\,\text{kHz}$ for $c = 1\,\text{mM}$ and $f > 1\,\text{MHz}$ for $c = 10\,\text{mM}$ in the case of Figure 2. This is in agreement with the linear dependence of the critical actuation frequency on the ion concentration
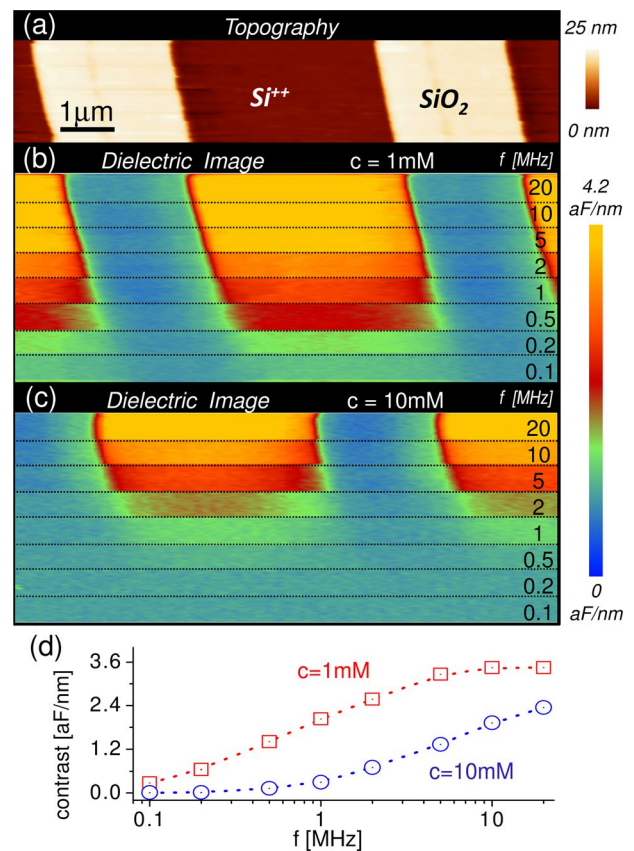

FIG. 2. (a) Topography and ((b) and (c)) dielectric contrast images ($\Delta C'$) of 20 nm thin and 2.5 μm wide Si^{++}/SiO_2 microstripes obtained in electrolyte solutions. Dielectric images were obtained at constant height Z = 100 nm from the Si^{++} baseline with ion concentrations $c = 1\,\text{mM}$ (b) and $c = 10\,\text{mM}$ (c) with $v_0 = 0.5\,\text{V}$. The applied frequency f was changed from 20 MHz to 0.1 MHz to show how the image contrast depends on the frequency and finally disappears at low frequencies. (d) Dielectric contrast ($\Delta C'$) extracted from images (b) and (c) as a function of the applied frequency. Dotted lines are to guide the eyes.

$f_{act} \sim c$ predicted by Eq. (2) based on the simple parallel-plate model.

As shown in Figure 2(d), the contrast increases with increasing frequency over two orders of magnitude until it plateaus at about 10 MHz for $c = 1$ mM and about 100 MHz (estimated) for $c = 10$ mM. This crossover is much smoother than is predicted by the parallel-plate model due to the complex probe geometry, but is in agreement with the simulations employing a more realistic geometry, as will be reported elsewhere.

Note that due to the high dielectric constant of water ($\varepsilon_{water} = 78$), the measured capacitance gradients are almost two orders of magnitude higher than those measured in air ($\varepsilon_{air} = 1$). This enables one to perform measurements with excellent signal-to-noise ratios while applying small voltages (here, $v_0 = 0.5$ V), as required to avoid electrochemical surface reactions.

The dielectric contrast of Figure 2 reflects both the dielectric properties of the materials and their topography. This is apparent from the force-distance curves in Figure 3 which were measured on the Si^{++} substrate and on a SiO$_2$ stripe at different frequencies (ion concentration of 1 mM).

It can be seen that the curves appear shifted by a relatively large distance, which can be shown to be of the order of $\sim h\varepsilon_{r,water}/\varepsilon_{r,sample}$, which clearly depends on both the dielectric constant of the sample and its thickness (topography).

To quantify the dielectric constants of the materials from the force-distance curves, we adapted the procedure that we previously used in air[13–15,21] to the case of a liquid environment of given conductivity and dielectric constant. First, for a given high frequency and given liquid properties, the probe geometry (R and θ) and the native oxide capacitance (C_{native}) were calibrated by fitting the numerical calculations to the approach curve measured on the Si^{++} substrate in electrolyte solution. Then, these parameters were used to fit the approach curve taken on the SiO$_2$ stripe with the relative permittivity of the oxide, ε_{r,SiO_2}, as the *single fitting parameter*. With this procedure, we obtained $R = 96$ nm, $\theta = 10°$, $C_{native} = 1.1\ \mu$F/cm^2, and $\varepsilon_{r,SiO_2} = 4.4 \pm 0.5$ for the measurements obtained at 20 MHz. While the soft Pt-tips became slightly blunter during the experiment, the values obtained are in good agreement with the nominal specifications of the probe ($R_{nom} \sim 30$ nm, $\theta_{nom} = 10°$–$30°$). Moreover, the dielectric properties of the native oxide, $C_{native,nom}$, and the SiO$_2$, $\varepsilon_{r,nom}$, are in excellent agreement with literature values for the bulk materials, which are 0.8–1.8 μF/cm^2 and 4, respectively, thus proving the method's excellent quantitative capabilities. The sensitivity of the results to the dielectric constant of the oxide structure is illustrated by the dashed lines in Figure 3, which correspond to the cases of $\varepsilon_{r,oxide} = 5.4$ and $\varepsilon_{r,oxide} = 3.4$. These results are robust to the choice of measurement frequency as can be seen in Figure 3 by the excellent agreement of the theoretical calculations with the experimental data for the frequency 5 MHz which were obtained with the parameters previously derived for 20 MHz *with no additional fitting parameters*. At lower frequencies, the agreement is still reasonable although some deviations between theoretical calculations and measurements start to appear. This is because at lower frequencies, the measurements become less local and include contributions from parts of the sample which are relatively far from the measuring point that are not included in the numerical modeling. These results unambiguously demonstrate that this technique can be used to measure the local dielectric constants of materials in electrolyte solutions.

In summary, we have demonstrated a technique that allows one to image and quantify the dielectric properties of materials in electrolyte solutions with nanometric spatial resolution. The technique presented can be easily implemented on commercially available AFMs and does not require major additional equipment or instrumentation changes. It opens a number of fascinating possibilities in fields such as electrophysiology and electrochemistry in which nanoscale dielectric information in electrolyte solutions is fundamental to understand a number of important phenomena.
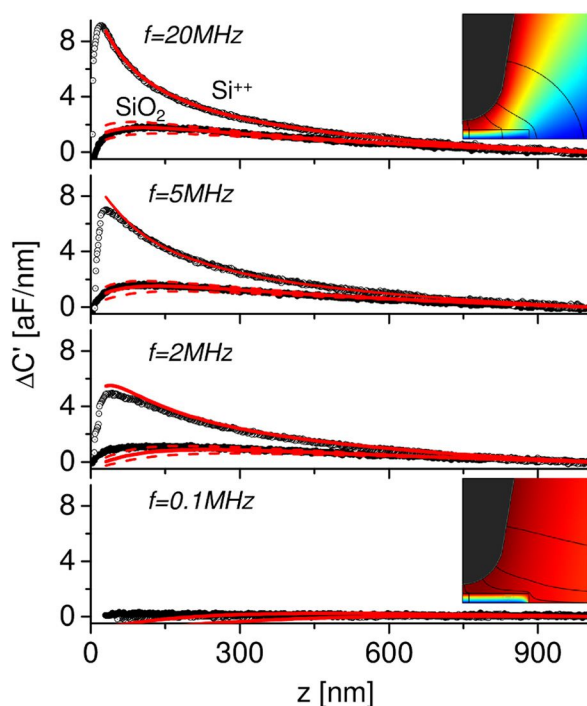

FIG. 3. (Symbols) Experimental approach curves onto the Si^{++} and the SiO$_2$ regions of the microstructure as a function of tip sample distance, z, measured at different frequencies in electrolyte solutions ($c = 1$ mM and $v_0 = 0.5$ V). Lines give the numerical results obtained with a probe with tip radius $R = 96$ nm, cone angle $\theta = 10°$, a native oxide capacitance $C_{native} = 1.1\ \mu$F/cm^2, and dielectric constant (solid) $\varepsilon_{r,oxide} = 4.4$, (dashed) $\varepsilon_{r,oxide} = 3.4$ and 5.4. Additional parameters of the numerical calculations: cone height $H = 10\ \mu$m, SiO$_2$ thickness $h = 20$ nm, and SiO$_2$ diameter $D = 3\ \mu$m. Insets show the simulated potential distributions for the probe apex held above the SiO$_2$ (20 MHz and 100 kHz). Electric field lines are shown in black.

[1]S. Scheuring, J. Seguin, S. Marco, D. Levy, B. Robert, and J. L. Rigaud, Proc. Natl. Acad. Sci. U.S.A. **100**, 1690 (2003).
[2]S. E. Cross, Y.-S. Jin, J. Rao, and J. K. Gimzewski, Nat. Nanotechnol. **2**, 780 (2007).

[3]J. V. Macpherson and P. R. Unwin, Anal. Chem. **72**, 276 (2000).

[4]S. Manne, P. K. Hansma, J. Massie, V. B. Elings, and A. A. Gewirth, Science **251**, 183 (1991).

[5]B. J. Rodriguez, S. Jesse, A. P. Baddorf, and S. V. Kalinin, Phys. Rev. Lett. **96**, 237602 (2006).

[6]M. P. Nikiforov, G. L. Thompson, V. V. Reukov, S. Jesse, S. Guo, B. J. Rodriguez, K. Seal, A. A. Vertegel, and S. V. Kalinin, ACS Nano **4**, 689 (2010).

[7]H. J. Butt, Biophys. J. **63**, 578 (1992).

[8]A. C. Hillier, S. Kim, and A. J. Bard, J. Phys. Chem. **100**, 18808 (1996).

[9]J. Sotres and A. M. Baro, Appl. Phys. Lett. **93**, 103903 (2008).

[10]Y. Hirata, F. Mizutani, and H. Yokoyama, Surf. Interface Anal. **27**, 317 (1999).

[11]N. Kobayashi, H. Asakawa, and T. Fukuma, Rev. Sci. Instrum. **81**, 123705 (2010).

[12]D. T. Lee, J. P. Pelz, and B. Bhushan, Nanotechnology **17**, 1484 (2006).

[13]L. Fumagalli, G. Ferrari, M. Sampietro, I. Casuso, E. Martinez, J. Samitier, and G. Gomila, Nanotechnology **17**, 4581 (2006).

[14]L. Fumagalli, G. Ferrari, M. Sampietro, and G. Gomila, Appl. Phys. Lett. **91**, 243110 (2007).

[15]L. Fumagalli, G. Ferrari, M. Sampietro, and G. Gomila, Nano Lett. **9**, 1604 (2009).

[16]J. Hu, X. D. Xiao, and M. Salmeron, Appl. Phys. Lett. **67**, 476 (1995).

[17]R. Shao, S. V. Kalinin, and D. A. Bonnell, Appl. Phys. Lett. **82**, 1869 (2003).

[18]L. S. Pingree and M. C. Hersam, Appl. Phys. Lett. **87**, 233117 (2005).

[19]C. Gao and X. D. Xiang, Rev. Sci. Instrum. **69**, 3846 (1998).

[20]W. Lu, D. Wang, and L. W. Chen, Nano Lett. **7**, 2729 (2007).

[21]G. Gramse, I. Casuso, J. Toset, L. Fumagalli, and G. Gomila, Nanotechnology **20**, 395702 (2009).

[22]L. Fumagalli, G. Gramse, D. Esteban-Ferrer, M. A. Edwards, and G. Gomila, Appl. Phys. Lett. **96**, 183107 (2010).

[23]T. L. Sounart, H. V. Panchawagh, and R. L. Mahajan, Appl. Phys. Lett. **96**, 203505 (2010).